Analyst

Accepted Manuscript

ROYAL SOCIETY OF CHEMISTRY

www.rsc.org/analyst

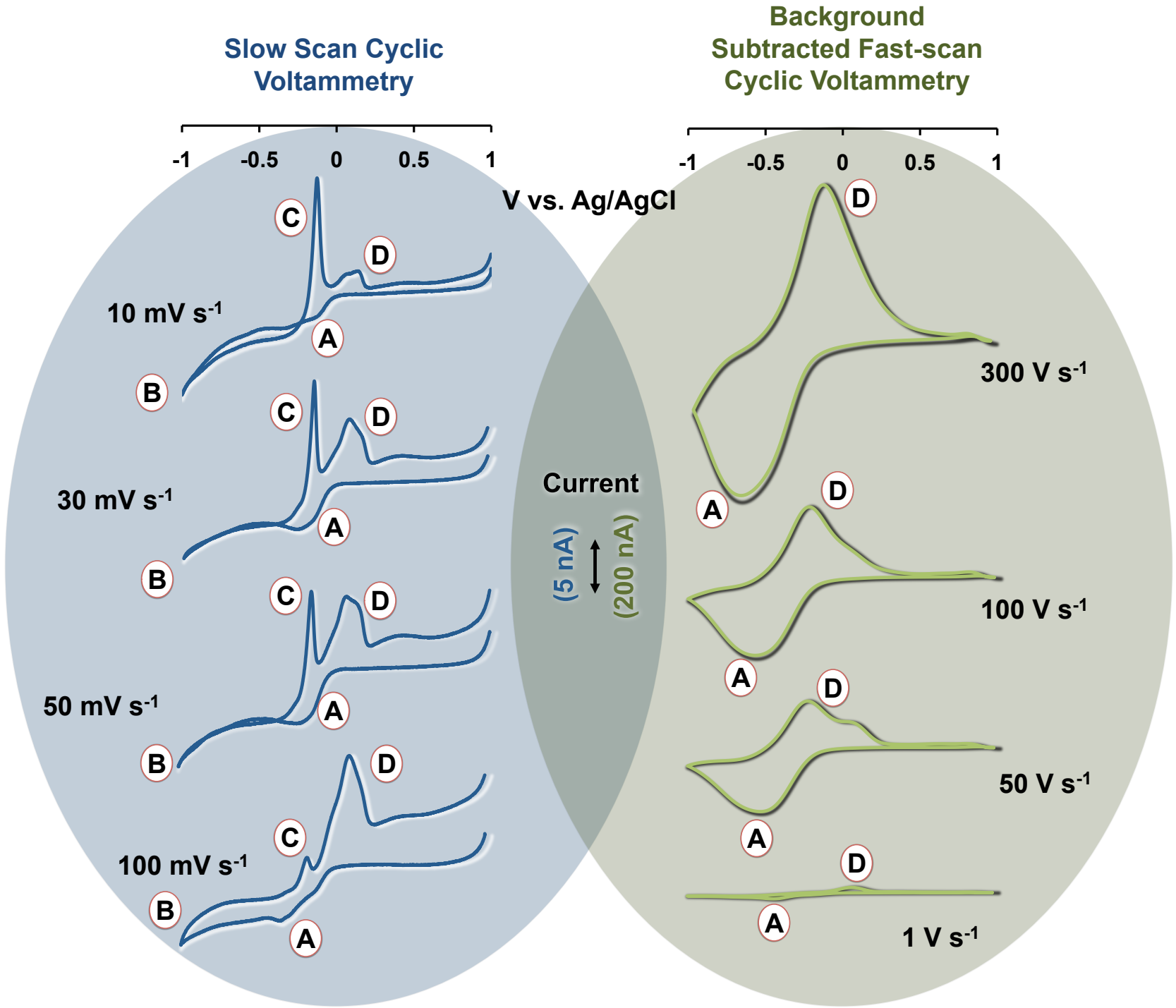

Fundamental studies of carbon fiber surfaces show that the rapid voltammetric response to trace metals is an adsorption driven process

The Analyst

RSCPublishing

ARTICLE

Fast Voltammetry of Metals at Carbon-Fiber Microelectrodes: Copper Adsorption onto Activated Carbon aids Rapid Electrochemical Analysis

Cite this: DOI: 10.1039/x0xx00000x

Received 00th January 2012,
Accepted 00th January 2012

DOI: 10.1039/x0xx00000x

www.rsc.org/

Pavithra Pathirathna[1], Srimal Samaranayake[1], Christopher W. Atcherley[2], Kate L. Parent[2], Michael L. Heien[2], Shawn P. McElmurry[3] and Parastoo Hashemi[1*]

Rapid, *in situ* trace metal analysis is essential for understanding many biological and environmental processes. For example, trace metals are thought to act as chemical messengers in the brain. In the environment, some of the most damaging pollution occurs when metals are rapidly mobilized and transported during hydrologic events (storms). Electrochemistry is attractive for *in situ* analysis, primarily because electrodes are compact, cheap and portable. Electrochemical techniques, however, do not traditionally report trace metals in real-time. In this work, we investigated the fundamental mechanisms of a novel method, based on fast-scan cyclic voltammetry (FSCV), that reports trace metals with sub-second temporal resolution at carbon-fiber microelectrodes (CFMs). Electrochemical methods and geochemical models were employed to find that activated CFMs rapidly adsorb copper, a phenomenon that greatly advances the temporal capabilities of electrochemistry. We established the thermodynamics of surface copper adsorption and the electrochemical nature of copper deposition onto CFMs and hence identified a unique adsorption-controlled electrochemical mechanism for ultra-fast trace metal analysis. This knowledge can be exploited in the future to increase the sensitivity and selectivity of CFMs for fast voltammetry of trace metals in a variety of biological and environmental models.

Introduction

Trace metal analysis in real-time is essential for understanding many biological and environmental processes. For example, trace metals have important functions in biology and are garnering new attention for their roles as neurotransmitters.[1, 2] In Alzheimer's disease for example, copper accumulates in β-amyloid plaques.[3] It is thought that this copper build-up comes at the expense of its normal roles as a neurotransmitter, accounting for some of the disease's neurological deficits.[3, 4] It has been impossible to chemically monitor endogenously acting copper to verify this hypothesis, primarily because chemical transmission occurs so quickly (< seconds).

Rapid metal analysis is also important in the environment, particularly in natural water systems where trace metal contamination is extremely hazardous.[5] The well-documented health consequences of trace metal exposure[6-9] are exacerbated because metals bioaccumulate in plants and animals,[10-13] providing numerous exposure paradigms for humans. Anthropogenic sources of trace metals are commonly mobilized and transported during hydraulic events (storms).[14] It is critical to characterize aquatic trace metals in real-time because their interactions with organic ligands and soils are fast (< seconds).[15] Such rapid metal detection would provide the most efficient implementation of existing metal mitigation systems [16-21] via a diagnostic approach.

Most analytical techniques cannot monitor metals rapidly (< seconds). Spectroscopic techniques are sensitive and selective, [22] however sample collection and preparation can alter metal speciation and make dynamic measurements difficult.[23, 24] Electrochemical methods are attractive because the chemistry occurs at a submersible or integrated surface that minimally impacts its surroundings. Ion-selective electrodes have a temporal resolution of seconds;[25, 26] however it is typically challenging to make measurements in dynamically changing matrices. Stripping voltammetries (such as anodic stripping and adsorptive stripping voltammetry) have extremely high sensitivities.[27] This high sensitivity is largely due to a lengthy pre-concentration step (minutes) that decreases temporal resolution.[28-30] Moreover, anodic stripping voltammetry is most commonly performed at Hg electrodes [31] which have limited portability and pose their own toxicity concerns.

We recently described the use of carbon-fiber microelectrodes (CFMs) to detect copper (II) (Cu^{2+}) and lead (II) (Pb^{2+}) with fast scan cyclic voltammetry (FSCV) at scan rates of 300 – 600 Vs^{-1}.[32, 33] Our ultra-fast, Hg-free method can quantify Cu^{2+} and Pb^{2+} concentration changes every 100 ms with parts per billion and parts per million sensitivity, respectively.[32, 33] Our method is highly applicable for studying metals in real time. However it is essential to describe the fundamental mechanisms of this fast voltammetric method before it can be developed into a routine analytical tool for biological and environmental applications. In this paper therefore, we take a multi-faceted approach and establish the underlying mechanisms of fast voltammetry of Cu^{2+} on CFMs in established laboratory test solutions.

We analyzed Cu^{2+}, a biologically relevant[2] and environmentally problematic metal ion[34] with well-known redox chemistry.[35, 36] Besides classical nucleation, growth and stripping features,[36] we observed new, additional peaks in Cu^{2+} slow scan cyclic voltammograms. These additional peaks were not diminished, as the classical features were, when the scan-rate was increased. In fact, with increasing scan rate, the new features were augmented, as seen previously with neurotransmitters adsorbed to CFM surfaces.[37] We therefore investigated surface adsorption as a fundamental mechanism of the Cu^{2+} FSCV signal. We utilized electrochemical, geochemical, and microscopic tools to describe CFM's surface and thermodynamic mechanisms towards Cu^{2+}. This study provides valuable insight into the adsorption chemistry that governs the FSCV response to metals. Our findings are critical to the future development of the method, namely increases in sensitivity and selectivity, in application to real samples.

Experimental Section

Solutions

Cu^{2+} solutions were prepared by dissolving $Cu(NO_3)_2$ in NaCl (0.01 M) and in tris buffer ((15 mM tris(hydroxymethyl)aminomethane), 140 mM NaCl, 3.25 mM KCl, 1.2 mM $CaCl_2$, 1.25 mM NaH_2PO_4, 1.2 mM $MgCl_2$ and 2.0 mM Na_2SO_4). All chemicals were purchased from Sigma-Aldrich (St. Louis, MO). At room temperature and pressure, the pH of Cu^{2+} in NaCl and tris buffer solutions was ~5.5 and 7.4 respectively.

Microelectrodes

CFMs were prepared by vacuum aspirating a single carbon fiber of 5 µm radius (T-650, Cytec Industries, NJ) into a glass capillary (0.6 mm external diameter, 0.4 mm internal diameter, A-M Systems, Inc., Sequim, WA). The capillary was pulled under gravity with a micropipette puller (Narishige, Tokyo, Japan) leaving a tapered end to form a carbon-glass seal. The exposed end of the carbon fiber was cut to approximately 150 µm under a microscope. Gold microelectrodes (AuMs) were prepared as described above but with a gold microwire of 10 µm radius (Goodfellow Co, PA), cut to approximately 150-200 µm.

Cyclic Voltammetry

All voltammetry employed a 2-electrode system. Cyclic voltammograms were collected on 5 different electrodes and representative examples are displayed. For slow scan cyclic voltammetry (scan rates ≤ 100 mVs^{-1}), microelectrodes were placed into a constantly stirred solution of $Cu(NO_3)_2$ and a triangular wave form (+1 V to –1 V) was applied using custom software, Wildcat CV, written in LAB-VIEW 2012 (National Instruments, Austin, TX). Only solutions for slow scan cyclic voltammetry were nitrogen-purged prior to experimentation. The reference electrode was fabricated by electroplating Cl^- on a Ag wire (A-M systems, WA). For scan rates above 1 Vs^{-1}, in-house software, WCCV 2.0, written in LABVIEW 2012 collected background-subtracted voltammograms in a flow-injection analysis system.

Electrochemical Pre-treatment

For most experiments microelectrodes were electrochemically pre-treated with a Cu^{2+} sensitive triangular waveform as previously described.[33] For experiments comparing electrochemical and chemical pretreatments, the anodic potential/rest potential of the CFMs was varied from +0.4 V to +1.3 V at a constant cathodic potential of -1.0 V at a scan rate of 300 Vs^{-1}. Electrodes were treated with each waveform for 10 minutes at 60 Hz and then 10 minutes at 10 Hz.

Chemical Pre-treatment

CFMs were chemically pretreated with a mixture of H_2SO_4 (0.25 M) and HNO_3 (0.25 M) in a 3:1 ratio[38] and washed with DI water prior to analysis.

Solution Geochemistry

Solution chemistry of Cu^{2+} in tris buffer and NaCl was modeled using PHREEQCi, a geochemical modeling software capable of determining speciation based on thermodynamic equilibrium. Stability constants during modeling were based on the MINTEQ.v4 database developed by the U.S. Environmental Protection Agency while additional constants for complexation with solutions were modeled in equilibrium with $CO_{2(g)}$ ($10^{-4.8}$ atm.) and $O_{2(g)}$ ($10^{-0.67}$ atm.).[39] The pH values predicted by PHREEQCi models were found to match the pH observed in experimental solutions.

Fast Scan Controlled-Adsorption Voltammetry (FSCAV)

A CFM was placed into a constantly stirred $Cu(NO_3)_2$ solution and a waveform (-1.0 V – +1.3 V, resting potential of 0 V, at 600 Vs^{-1}) was applied. An electronic relay (ADG-419, Analog Devices) was used to switch between the applied waveform and a constant potential of 0 V for 10 seconds to allow copper adsorption at the electrode surface reach equilibrium. After 10 seconds, the waveform was reapplied, and the first background-subtracted cyclic voltammogram was collected and analyzed for total adsorbed copper. In house LabVIEW 2012 software integrated the reduction peak from the background subtracted cyclic voltammogram of Cu^{2+} and Faraday's law was used to convert this to a surface concentration (Γ_{Cu}). Measured data was fit to the linearized Langmuir isotherm (eq. 1) where C is the [Cu^{2+}] in bulk solution, Γ_{max} is the maximum monolayer surface coverage, and K is the

equilibrium constant for adsorption. This experiment was performed in NaCl (10 mM) and tris buffer (15 mM).

$$c\Gamma_{Cu} = \frac{1}{\Gamma_{Max}}c + \frac{1}{\Gamma_{Max}K} \quad (1)$$

Atomic Force Microscopy (AFM)

CFMs were prepared as described above and electrochemically activated. During slow scan cyclic voltammograms of $Cu(NO_3)_2$ (100 µM) (from +1 V to -1 V , back to +1 V), electrodes were temporarily disconnected for groups of electrodes at 6 different points. Those were 0.2, -0.6 and -1 V on the forward scan and -0.6, -0.3 and 0.2 V on the reverse scan, all vs. Ag/AgCl. These electrodes had been exposed only to a partial section of the waveform. Electrodes were stored in a closed container and transported to the AFM. AFM images were taken using a Park Systems XE-NSOM instrument with a non-contact tip.

Results and Discussion

Slow Scan Cu^{2+} Cyclic Voltammetry at CFMs

During slow-scan Cu^{2+} cyclic voltammetry, a cathodic potential sweep is applied to the electrode at 1 – 10 mVs^{-1}, followed by an anodic sweep that brings the potential back to rest.[36] During the cathodic scan, copper is deposited on the electrode surface following a nucleation and growth mechanism. Copper nucleates over a broad potential range. These nuclei allow more Cu to deposit during a growth phase at any potential sufficient for deposition. Therefore, there are often two broad 'loop' reduction peaks, between the same voltages, on both cathodic and anodic scans.[36] The differences between the nature of the electrode surface and the Cu surface make this nucleation/growth deposition occur at a more negative voltage than the standard Cu^{2+} reduction potential.[40, 41] Indeed when holding a CFM at a constant potential of 0.34 V (Cu^{2+} $2e^- \rightarrow Cu_{(s)}$ standard reduction potential), addition of $Cu(NO_3)_2$ induced no change in current. This behavior is true for holding potentials down to -0.1 V (data not shown). During the anodic scan, the deposited $Cu_{(s)}$ is stripped off the electrode surface. Because this happens from a $Cu_{(s)}$ rich surface (a single phase), the stripping or oxidation peak is sharp and its voltage is much closer to the standard equilibrium potential.[40, 41] Metal deposition can also occur via other mechanisms, for example, adsorption, charge transfer, and under potential deposition (UPD).[42-44] UPD is a process by which a metal deposits onto another metal at a more positive electrode potential than the Nernst potential for bulk deposition.[42]

CFM slow scan cyclic voltammetry of Cu^{2+} was probed here by comparisons to AuMs. **Figure 1** shows representative cyclic voltammograms of $Cu(NO_3)_2$ (100 µM) on a Au Microelectrode (AuM) **(a)** and a CFM **(b)** at 10 mVs^{-1} in NaCl. These two voltammograms share common features. For example, Cu^{2+} reduction to metallic Cu begins at -0.1 V (peaks A', A) and continues via a loop formation between -0.4 V and -1.0 V on the cathodic scans (peaks B', B). This loop formation is an indication of nucleation and growth processes and is similar to previous observations.[43] On both AuMs and CFMs, sharp stripping peaks (C', C) and shoulder peaks (D', D) are present between -0.1 to 0.2 V on the anodic scans. Shoulders accompanying stripping peaks have previously been reported on glassy carbon electrodes [44] and highly oriented pyrolytic graphite electrodes.[43] The presence of complexing agents such as chloride and ammonia strongly affect copper redox processes and lead to the observation of shoulder peaks at potentials higher than stripping peaks.[41, 43-47] Shoulder peaks have not been found to be associated with stripping peaks in media containing no complexing agents. [40, 48-51]

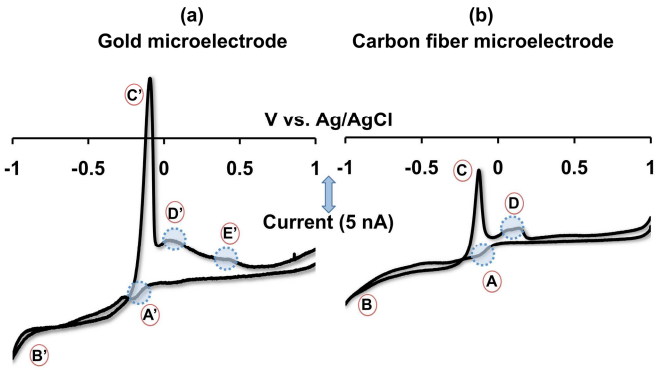

Figure 1. Slow scan cyclic voltammograms of $Cu(NO_3)_2$ on (a) AuM and (b) CFM at a scan rate of 10 mVs^{-1} in NaCl. Peaks A' – E' appear on the AuM, whereas peaks A – D appear on the CFM.

A mechanism for shoulder peak formation in the presence of Cl^- has been speculated previously.[44, 47, 49] First, deposited Cu oxidizes to Cu^+, creating a stripping peak (C', C) and forming a barely conductive, passive layer of CuCl according to reaction (2).

$$Cu + Cl^- \rightarrow CuCl + e^- \quad (2)$$

The CuCl layer shields underlying metallic copper thereby momentarily arresting further oxidation. Dissolution of this passive layer occurs either via direct diffusion or diffusion of a more soluble complex (such as $CuCl_2^-$). Dissolution exposes the remaining underlying metal allowing the electro-oxidation of Cu to continue as shown in reactions (3) and (4):

$$CuCl + Cl^- \rightarrow CuCl_2^- \quad (3)$$

$$CuCl_2^- \rightarrow Cu^{2+} + 2Cl^- + e^- \quad (4)$$

We determined whether these processes are responsible for shoulder peaks D' and D by systematically increasing the scan rate as described in the next section. There is an additional peak on the AuM that is not present on the CFM (peak E'). UPD plays a significant role in copper deposition on gold surfaces [42] whereas on carbon materials, metallic copper follows bulk deposition with no evidence for UPD.[41, 43, 44, 46, 49, 53] Peak E' on the AuM is likely a consequence of anodic processes associated with UPD on gold.[42]

Scan Rate Dependence

The shoulder peak mechanism proposed above was tested on CFMs by progressively increasing scan rate. The rationale here is that by increasing scan rate, nucleation/growth and hence stripping become

limited because these processes are mass-transport dependent.[41] Because reactions (3) and (4) rely on the stripping peak, any limitations in stripping should manifest proportionally on the shoulder peak.

In this experiment cyclic voltammograms of $Cu(NO_3)_2$ were collected at CFMs at increasing scan rates. From 10 – 100 mVs^{-1}, raw traces were analyzed; however at higher scan rates, the charging current due to double layer capacitance dominates the Faradaic component of the voltammetric signal. Therefore, cyclic voltammograms at 1 Vs^{-1} and above were collected in a flow injection system (FIA) using background subtraction.

Figure 2 shows cyclic voltammograms collected at 10, 30, 50 and 100 mVs^{-1} (left, blue panel) and at 1, 50, 100 and 300 Vs^{-1} (right, green panel). This experiment illustrates the evolution of a slow scan $Cu(NO_3)_2$ cyclic voltammogram in a typical FSCV signal.[33] Increased peak separation at high FSCV scan rates is due to slow electron transfer kinetics. All peaks are labeled as in **Figure 1**. From 10 – 100 mVs^{-1}, the magnitude of peaks (B) and (C) are greatly reduced such that they are almost absent at 100 mVs^{-1}. This is consistent with the notion that nucleation and growth are mass-transport limited and therefore can be 'outrun' at high scan rates. The magnitude of peaks (A) and (D) however are not subject to the same behavior. Peaks (A) and (D) are present and well defined at 100 mVs^{-1} implying that these features are neither mass-transport limited nor dependent on peaks (B) and (C). The results of these experiments indicate that mechanisms other than those described by Reactions (3) and (4) are responsible for peak (D).

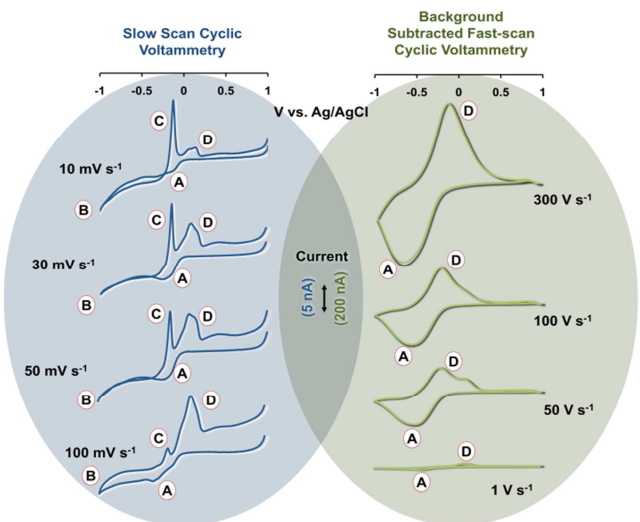

Figure 2. Left: Slow scan cyclic voltammograms of $Cu(NO_3)_2$ on CFMs at scan rates of 10, 30, 50 and 100 mVs^{-1}. Right: Fast scan background-subtracted cyclic voltammograms of $Cu(NO_3)_2$ at scan rates of 1, 50, 100 and 300 Vs^{-1}.

For adsorbed species, the peak current is proportional to scan rate[51] and we indeed found that from 1 – 300 Vs^{-1}, peak amplitudes increased. Furthermore, the slope of a plot of the log current vs. log scan rate for $Cu(NO_3)_2$ was previously reported to be approximately 1 at high scan rates.[33] Taken together, these findings strongly support a hypothesis that peaks (A) and (D) stem from an adsorption controlled process. Adsorption is explored in the following sections.

CFM Over-oxidation Leads to Enhanced Sensitivity

Activated carbon is widely used in wastewater treatment and is the primary purification component of domestic water filters.[52, 53] When carbon is activated (e.g. via heat in the presence of air, or with chemical or electrochemical pretreatments) a wide array of oxygen functionalities are created on its surface.[54] These oxygen moieties adsorb and complex trace metals, removing them from solution.[54, 55]

CFMs are typically electrochemically pre-treated prior to use.[56] Therefore, in analogy to metal adsorption by activated carbon, the oxygen functionalities on the CFM surface may rapidly complex trace metals in solution, pre-concentrating them on the surface. In this experiment, we tested the hypothesis that enhanced surface oxidation is responsible for increased FSCV sensitivity towards Cu^{2+}, presumably due to an increased number of adsorption sites.

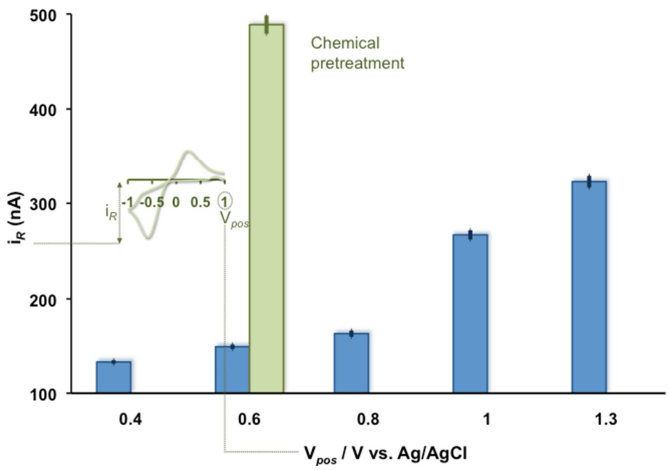

Figure 3. Maximum cathodic current of $Cu(NO_3)_2$ (10 µM) fast scan cyclic voltammograms as a function of anodic potential limit (blue series) at 300 Vs^{-1} and as a function of acid pretreatment (green).

Using flow injection analysis, we collected background subtracted cyclic voltammograms of CFMs exposed to a bolus of $Cu(NO_3)_2$ (10 µM) with different FSCV waveforms. We systematically increased the anodic potential limit of the waveform at a constant cathodic limit, -1.0 V. Figure 3 shows the magnitude of cathodic current (demonstrated by the inset cyclic voltammogram) as a function of the anodic potential limit. The cathodic current showed exponential increases with increasing anodic potential. This exact behavior was previously reported with neurotransmitters and attributed to surface 'activation' or over-oxidation.[56] To confirm that the enhanced sensitivity was due to over-oxidation, an alternative method to over-oxidize the CFM surface was employed. An acid pretreatment [38] was applied to the electrode surface prior to use (H_2SO_4 (0.25 M) and HNO_3 (0.25 M) in a 3:1 ratio). An anodic potential limit of +0.6 V was used where we previously found negligible effects of electrochemical over-oxidation. The resultant cathodic current is plotted in green on the 0.6 V series. The current here is substantially higher than the non-acid treated CFM confirming that surface activation, by two separate means, begets similar outcomes.

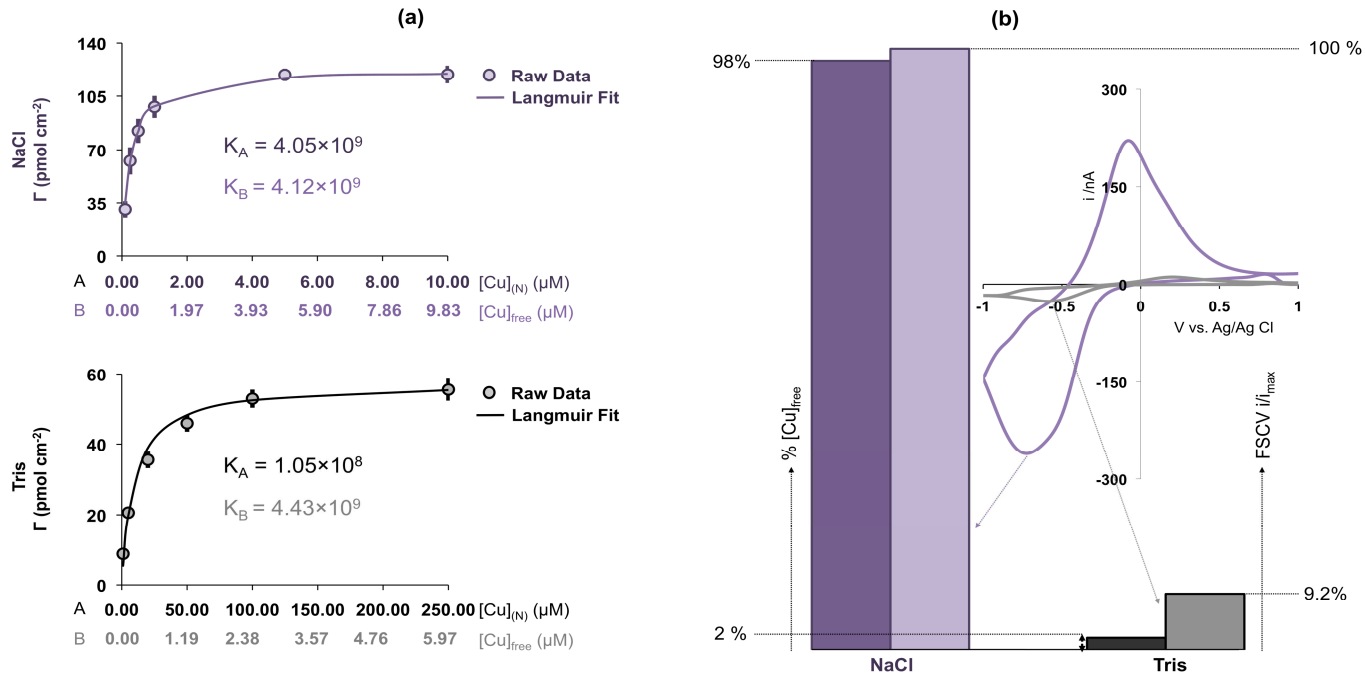

Figure 4. (a) Langmuir adsorption isotherms for $Cu(NO_3)_2$ on CFMs in NaCl (top) and in tris buffer (bottom). (b) Histogram showing % $[Cu^{2+}]_{free}$ in solution and % cathodic current of $Cu(NO_3)_2$ (10 μM) in NaCl (purple series) and in tris buffer (black series) at 300 Vs^{-1} (% cathodic current is shown by setting the maximum cathodic current with tris buffer to 100% and expressing the cathodic current with NaCl as a percentage of this). The inset background-subtracted cyclic voltammograms are representative examples taken in NaCl (purple) and tris buffer (black)

Cu^{2+} Adsorption to CFMs drives the FSCV Signal

We sought to verify that the enhanced FSCV sensitivity towards Cu^{2+} as a consequence of activation is an adsorption-driven mechanism. This was successfully confirmed by construction of adsorption isotherms using fast scan controlled-adsorption voltammetry (FSCAV) on CFMs.[57] Adsorption isotherms describe the thermodynamic equilibrium of Cu^{2+} onto the CFM, providing an index of the amount of Cu^{2+} on the CFM surface with respect to bulk solution via the equilibrium constant, K.

In all experiments described above, we used a simple matrix, NaCl, for characterizations. The adsorption isotherm of Cu^{2+} on CFMs in NaCl is shown in **Figure 4a (top panel)** and follows a Langmuir fit. Authentic biological and environmental matrices are more complicated than NaCl and contain copper binding components. Therefore, we studied whether a complex matrix would affect Cu^{2+} adsorption. We previously characterized copper in tris buffer[33] which has considerable metal binding capacity, [58,59]. Additionally Tris acts as a model biological medium because it contains amines that mimic proteins. The other salts in the buffer are at a ratio and concentration designed to mimic artificial cerebrospinal fluid (ACSF). Many neurotransmitters and other biologically relevant molecules have been characterized in tris *in vitro*[60-62] therefore adsorption isotherms were additionally constructed in tris buffer, (**Figure 4a bottom)** also following a Langmuir fit.

We previously used a geochemical model to calculate the equilibrium concentrations of free Pb^{2+} in test solutions.[32] We employed the same model here to calculate free Cu^{2+} concentration ($[Cu^{2+}]_{free}$) in NaCl and tris solutions. Our isotherms therefore have two x-axes, (A) denotes the concentration of Cu^{2+} added ($[Cu^{2+}]_{(N)}$) to the test solutions and (B) denotes the free Cu^{2+} concentration $[Cu^{2+}]_{free}$ in solution. For NaCl, the two x-axes values are similar because NaCl has little Cu^{2+} binding capacity. Therefore when calculating K, there is little difference between the values calculated with $[Cu^{2+}]_{(N)}$ vs. $[Cu^{2+}]_{free}$ (K_A and K_B). For tris the values of axes (A) and (B) are dramatically different because tris has Cu^{2+} binding capacity with K ~ 10^4.[59] It is interesting however, that when $[Cu^{2+}]_{free}$ is taken into consideration in the calculation, K (K_B) is similar to the K values in NaCl. Therefore, this complex matrix does not affect the monolayer characteristics of Cu^{2+} adsorption onto CFMs. This experiment further shows that solution complexes and other species do not significantly adsorb to the CFM surface and alter K.

The interactions of the Cu^{2+}- CFM and Cu^{2+} - tris equilibria are complicated. **Figure 4b** is a histogram that compares % $[Cu^{2+}]_{free}$ in solution to the cathodic current of background subtracted cyclic voltammograms of $Cu(NO_3)_2$ in NaCl (purple series) and tris buffer (black series). Shown in the inset are representative examples of cyclic voltammograms of $Cu(NO_3)_2$ in NaCl and tris buffer. In the histogram, we compared the two FSCV signals thus: the maximum

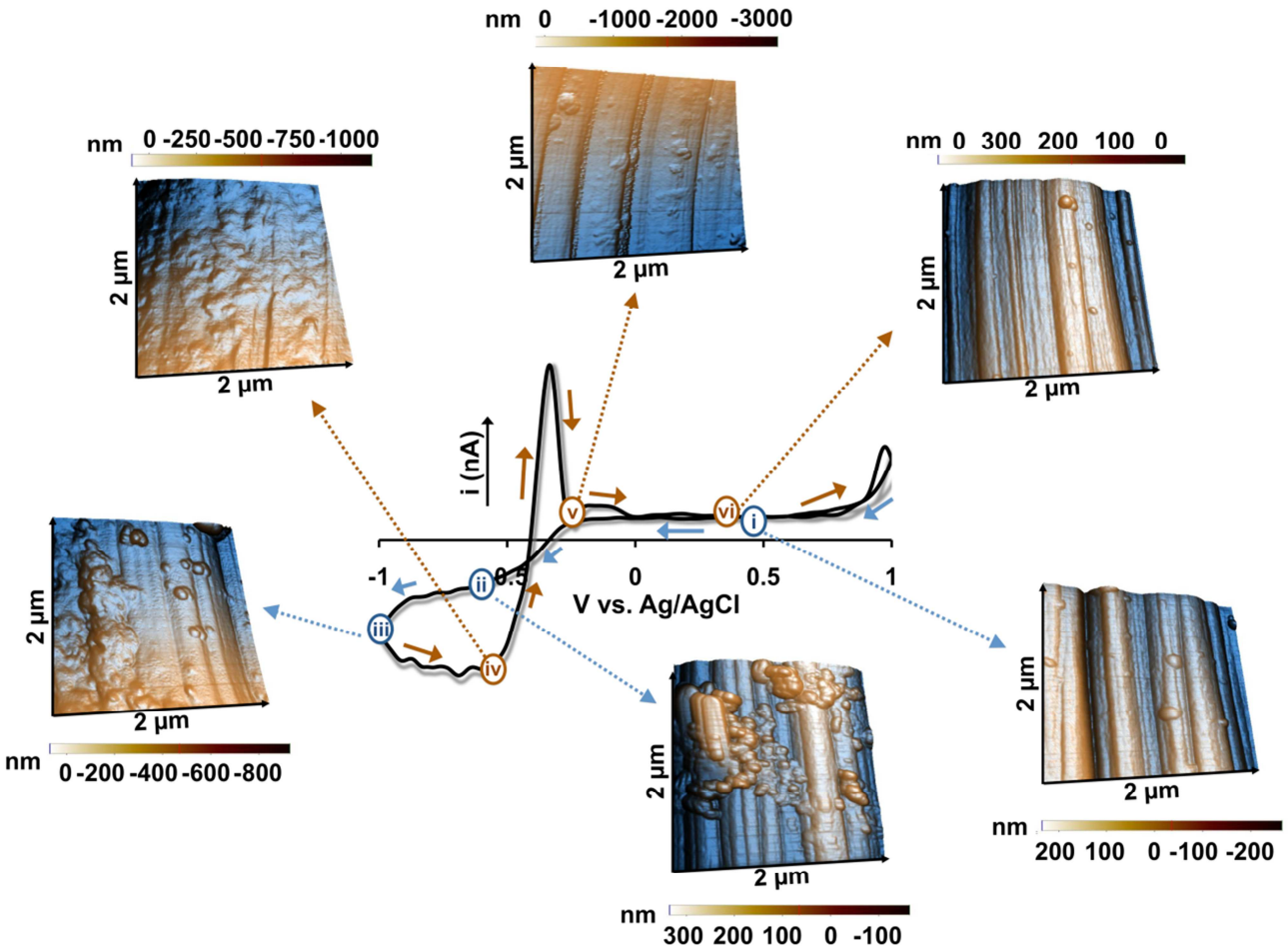

Figure 5. AFM images of a slow scan (10 mVs^{-1}) cyclic voltammogram of $Cu(NO_3)_2$ (100 µM) in tris buffer taken at six different points along the scan. On the forward scan, images were recorded at 0.2 V (i), -0.6 V (ii) and -1 V (iii) and on the backward scan at 0.6 V (iv), -0.3 V (v) and 0.2 V (vi). AFM images are 2 µM x 2 µM.

cathodic current with tris buffer was normalized to 100% and the current with NaCl was expressed as a percentage of this. It is seen that despite only 2% $[Cu^{2+}]_{free}$ in tris buffer, that the Cu^{2+} signal is 9.2% of the Cu^{2+} signal in NaCl (with 98% $[Cu^{2+}]_{free}$). This discrepancy implies that the two equilibria compete. The equilibrium of Cu^{2+}- CFM complexation is more favorable than Cu^{2+} - tris complexation, and a serendipitous outcome of this effect is high FSCV sensitivity, even in Cu^{2+} complexing matrices.

Given the confirmation that our Cu^{2+} FSCV signal is highly adsorption driven, the nucleation characteristics of the cyclic voltammetry peaks on CFMs were next studied.

AFM Characterization of Cu Nucleation and Oxidation

Changes in the morphology of the CFM surface can be visualized with AFM. AFM is a sensitive surface imaging technique, which employs a cantilevered tip to convert surface contours into images. AFM is routinely used to establish and characterize the formation of metallic copper on electrode surfaces.[40, 41] In **Figure 5**, AFM images were recorded at six different points along a slow scan cyclic voltammogram of $Cu(NO_3)_2$ in a complex matrix, tris buffer. Shortly after the start of the scan (i) the striations of the bare CFM surface are well defined. The small round features on the surface are likely solid contaminants. At (ii), metallic copper clusters are present on the CFM surface showing that the eventual cathodic FSCV peak (which evolves from this peak at high scan rates) involves deposition of $Cu_{(s)}$. $Cu_{(s)}$ is more elaborate during nucleation (iii) and after growth (iv) where striations are no longer visible under metallic Cu. After stripping (v), striations are again visible and due to the removal of metallic Cu. During the stripping process, $Cu_{(s)}$ may either be oxidized to Cu^{+} (as discussed above) or directly to Cu^{2+}. The presence of clear carbon striations and the scan rate dependent data provide little evidence for the formation of CuCl. However, the nature of the peak directly proceeding the stripping peak (the eventual anodic FSCV anodic peak) is yet to be determined. One explanation is that this $Cu_{(s)}$ is deposited on specific CFM adsorption sites that have their own discrete oxidation potentials. The remaining clusters are no longer present at point (vi), confirming that $Cu_{(s)}$ is completely oxidized at the end of the scan.

These surface morphology data confirm the nucleation and oxidation of metallic Cu associated with the cathodic and anodic FSCV peaks,

i.e., peaks A and B in the FSCV segment of **Figure 2** are due to $Cu^{2+} + 2\ e^- \rightarrow Cu_{(s)}$ and the reverse reaction.

Conclusion

FSCV at CFMs is an excellent tool for fast metal analysis with essential applications in biology and the environment. In this work, we described the fundamental mechanisms of fast scan voltammetry of Cu^{2+} on CFMs. In analogy to metal remediation by activated carbon, we showed that adsorption on CFMs underlies rapid FSCV responses. We ascertained the thermodynamic and physical characteristics of the CFM adsorption mechanism. This study has allowed us to understand the fundamentals of Cu^{2+} FSCV, enabling future improvements in the sensitivity and selectivity of fast metal voltammetry for real-time biological and environmental analysis.

Acknowledgements

The authors thank Chris Thrush for technical assistance with AFM and XPS. Audrey Sulkanen for technical assistance with carbon-fiber microelectrodes. Prof. Martyn Boutelle, Prof. Mark Meyeroff and Dr. Tooraj Hashemi for helpful conversations. WSU's President's Research Enhancement Award and University of Arizona funded this research.

Notes and references

[a] *Department of Chemistry, Wayne State University, 5101 Cass Avenue, Detroit, MI 48202,USA*
[b] *Department of Chemistry and Biochemistry, University of Arizona, 1306 East University Blvd., Tucson, AZ 85721*
[c] *Department of Civil and Environmental Engineering, Wayne State University, 5050 Anthony Wayne Drive, Detroit, MI 48202*

** To whom correspondence should be addressed: phashemi@chem.wayne.edu*

1. E. D. Gaier, B. A. Eipper and R. E. Mains, *J Neurosci Res*, 2013, 91, 2-19.
2. E. L. Que, D. W. Domaille and C. J. Chang, *Chem Rev*, 2008, 108, 1517-1549.
3. Y. H. Hung, A. I. Bush and R. A. Cherny, *J Biol Inorg Chem*, 2010, 15, 61-76.
4. I. G. Macreadie, *Eur Biophys J*, 2008, 37, 295-300.
5. K. Haarstad, H. J. Bavor and T. Maehlum, *Water Sci Technol*, 2012, 65, 76-99.
6. E. Vaiopoulou and P. Gikas, *Water Res*, 2012, 46, 549-570.
7. L. M. Chiodo, S. W. Jacobson and J. L. Jacobson, *Neurotoxicol Teratol*, 2004, 26, 359-371.
8. S. Charlesworth, E. De Miguel and A. Ordonez, *Environ Geochem Health*, 2011, 33, 103-123.
9. G. J. Brewer, *Clin Neurophysiol*, 2010, 121, 459-460.
10. E. Islam, X. E. Yang, Z. L. He and Q. Mahmood, *J Zhejiang Univ Sci B*, 2007, 8, 1-13.
11. J. R. Peralta-Videa, M. L. Lopez, M. Narayan, G. Saupe and J. Gardea-Torresdey, *Int J Biochem Cell Biol*, 2009, 41, 1665-1677.
12. D. M. Ward, K. H. Nislow and C. L. Folt, *Annals of the New York Academy of Sciences*, 2010, 1195, 62-83.
13. S. Balshaw, J. Edwards, B. Daughtry and K. Ross, *Rev Environ Health*, 2007, 22, 91-113.
14. C. M. Dean, J. J. Sansalone, F. K. Cartledge and J. H. Pardue, *J. Environ. Eng.-ASCE*, 2005, 131, 632-642.
15. D. G. Strawn and D. L. Sparks, *Soil Science Society of America Journal*, 2000, 64, 144-156.
16. N. E. Selin, *J Environ Monit*, 2011, 13, 2389-2399.
17. L. Ritter, K. Solomon, P. Sibley, K. Hall, P. Keen, G. Mattu and B. Linton, *Journal of Toxicology and Environmental Health-Part a-Current Issues*, 2002, 65, 1-142.
18. R. W. Peters, *J Hazard Mater*, 1999, 66, 151-210.
19. J. Kumpiene, A. Lagerkvist and C. Maurice, *Waste Manag*, 2008, 28, 215-225.
20. H. Brix, *Water Science and Technology*, 1999, 40, 45-50.
21. R. H. Kadlec and S. D. Wallace, *Treatment Wetlands*, CRC Press, Boca Ranton, 2nd edn., 2009.
22. O. T. Butler, W. R. L. Cairns, J. M. Cook and C. M. Davidson, *Journal of Analytical Atomic Spectrometry*, 2012, 27, 187-221.
23. H. M. Anawar, *Talanta*, 2012, 88, 30-42.
24. K. Fytianos, *J AOAC Int*, 2001, 84, 1763-1769.
25. E. Pretsch, *Trac-Trends in Analytical Chemistry*, 2007, 26, 46-51.
26. E. Bakker, E. Pretsch and P. Buhlmann, *Anal Chem*, 2000, 72, 1127-1133.
27. X. Dai, O. Nekrassova, M. E. Hyde and R. G. Compton, *Anal Chem*, 2004, 76, 5924-5929.
28. M. L. Tercier-Waeber, J. Buffle, F. Graziottin and M. Koudelka-Hep, *Abstracts of Papers of the American Chemical Society*, 2000, 220, U317-U317.
29. A. M. A. Mota, J. Buffle, S. P. Kounaves and M. L. S. Goncalves, *Analytica Chimica Acta*, 1985, 172, 13-30.
30. J. H. Pei, M. L. Tercier-Waeber and J. Buffle, *Analytical Chemistry*, 2000, 72, 161-171.
31. J. Barek, A. G. Fogg, A. Muck and J. Zima, *Critical Reviews in Analytical Chemistry*, 2001, 31, 291-309.
32. Y. Yang, P. Pathirathna, T. Siriwardhane, S. P. McElmurry and P. Hashemi, *Anal Chem*, 2013, 85, 7535-41
33. P. Pathirathna, Y. Yang, K. Forzley, S. P. McElmurry and P. Hashemi, *Anal Chem*, 2012, 84, 6298-6302.
34. L. Kiaune and N. Singhasemanon, *Rev Environ Contam Toxicol*, 2011, 213, 1-26.
35. M. E. Hyde and R. G. Compton, *Journal of Electroanalytical Chemistry*, 2003, 549, 1-12.
36. C. Prado, S. J. Wilkins, F. Marken and R. G. Compton, *Electroanalysis*, 2002, 14, 262-272.
37. R. B. Keithley, P. Takmakov, E. S. Bucher, A. M. Belle, C. A. Owesson-White, J. Park and R. M. Wightman, *Anal Chem*, 2011, 83, 3563-3571.
38. E. J. Parra, P. Blondeau, G. A. Crespo and F. X. Rius, *Chem Commun*, 2011, 47, 2438-2440.
39. A. G. Aslamkhan, A. Aslamkhan and G. A. Ahearn, *Journal of Experimental Zoology*, 2002, 292, 507-522.
40. B. Pesic and D. Grujicic, *Electrochimica Acta*, 2002, 47, 2901-2912.
41. D. Grujicic and B. Pesic, *Electrochimica Acta*, 2005, 50, 4426-4443.
42. D. Krznaric and T. Goricnik, *Langmuir*, 2001, 17, 4347-4351.
43. R. Srinivasan and P. Gopalan, *Surf Sci*, 1995, 338, 31-40.
44. K. Shi, K. Hu, S. Wang, C. Y. Lau and K. K. Shiu, *Electrochimica Acta*, 2007, 52, 5907-5913.

45. D. E. Garcia-Rodriguez, L. H. Mendoza-Huizar, C. H. Rios-Reyes and M. A. Alatorre-Ordaz, *Quimica Nova*, 2012, 35, 699-704.
46. C. Nila and I. Gonzalez, *Journal of Electroanalytical Chemistry*, 1996, 401, 171-182.
47. K. Yoo, B. Miller, X. Shi and R. Kalish, *Journal of the Electrochemical Society*, 2001, 148, C95-C101.
48. L. Huang, E. S. Lee and K. B. Kim, *Colloids and Surfaces a-Physicochemical and Engineering Aspects*, 2005, 262, 125-131.
49. G. G. Lang, M. Ujvari and G. Horanyi, *Journal of Electroanalytical Chemistry*, 2002, 522, 179-188.
50. J. J. Lee, B. Miller, X. Shi, R. Kalish and K. A. Wheeler, *Journal of the Electrochemical Society*, 2001, 148, C183-C190.
51. A. J. Bard and L. R. Faulkner, *Electrochemical Methods - Fundamentals and Applications*, JOHN WILEY & SONS, INC., New York, Second edn., 2000.
52. M. O. Corapcioglu and C. P. Huang, *Water Research*, 1987, 21, 1031-1044.
53. D. Mohan and C. U. Pittman, Jr., *J Hazard Mater*, 2006, 137, 762-811.
54. M. Seredych, D. Hulicova-Jurcakova, G. Q. Lu and T. J. Bandosz, *Carbon*, 2008, 46, 1475-1488.
55. S. Biniak, M. Pakula, G. S. Szymanski and A. Swiatkowski, *Langmuir*, 1999, 15, 6117-6122.
56. M. L. Heien, P. E. Phillips, G. D. Stuber, A. T. Seipel and R. M. Wightman, *The Analyst*, 2003, 128, 1413-1419.
57. C. W. Atcherley, N. D. Laude, K. L. Parent and M. L. Heien, *Langmuir*, 29, 14885-14892.
58. D. McPhail and B. Goodman, *Biochemical Journal*, 1984, 221, 559.
59. J. Nagaj, K. Stokowa-Soltys, E. Kurowska, T. Fraczyk, M. Jezowska-Bojczuk and W. Bal, *Inorg Chem*, 2013, 52, 13927-13933.
60. P. Hashemi, E. C. Dankoski, J. Petrovic, R. B. Keithley and R. M. Wightman, *Analytical Chemistry*, 2009, 81, 9462-9471.
61. A. E. Ross and B. J. Venton, *Analyst*, 2012, 137, 3045-3051.
62. J. G. Roberts, K. L. Hamilton and L. A. Sombers, *Analyst*, 2012, 136, 3550-3556.